Proof-of-Concept Demonstration of Vector Beam Pattern Measurements of Kinetic Inductance Detectors

Davis, Kristina K.; Jellema, Willem; Yates, Stephen J. C.; Ferrari, Lorenza; Baselmans, Jochem J. A.; Kohno, Kotaro; Thoen, David; Murugesan, Vignesh; Baryshev, Andrey M.

Published in:
Ieee transactions on terahertz science and technology

DOI:
10.1109/TTHZ.2016.2617869

Publication date:
2017

Proof-of-Concept Demonstration of Vector Beam Pattern Measurements of Kinetic Inductance Detectors

Kristina K. Davis, Willem Jellema, Stephen J. C. Yates, Lorenza Ferrari, Jochem J. A. Baselmans, Kotaro Kohno, David Thoen, Vignesh Murugesan, and Andrey M. Baryshev

***Abstract*—We present results from the first vector beam pattern measurement of microwave kinetic inductance detectors (MKIDs). Vector beam patterns require sampling of the E-field of the receiver in both amplitude and phase. MKIDs are inherently direct detectors and have no phase response to incoming radiation. We map the amplitude> and phase patterns of the detector beam profile by adapting a two-source heterodyne technique. Our testing strategy recovers the phase information by creating a reference signal to trigger data acquisition. The reference is generated by mixing the slightly offset low-frequency signals from the output of the two synthesizers used to drive the submillimeter sources. The key requirement is that the time-series record always begins at the same set phase of the reference signal. As the source probe is scanned within the receiver beam, the wavefront propagation phase of the receiver changes and causes a phase offset between the detector output and reference signals. We demonstrated this technique on the central pixel of a test array operating at 350 GHz. This methodology will enable vector beam pattern measurements to be performed on direct detectors, which have distinct advantages reducing systematic sources of error, allowing beam propagation, and removing the far-field measurement requirement such that complicated optical systems can be measured at a point that is easily accessible, including the near field.**

***Index Terms*—Direct detector, kinetic inductance detector (KID), phase response, radiation pattern, vector beam pattern.**

I. Background

Microwave kinetic inductance detectors (MKIDs) measure the change in kinetic inductance of a superconducting resonator upon photon absorption, causing a detectable phase shift in the detector readout [1]–[3]. This process is sensitive only to the total power of the incident electric field, therefore, kinetic inductance detectors (KIDs) are direct detectors (phase insensitive). Typical beam pattern characterization, relies on scalar (amplitude only) detection of a source scanned in the main beam of the receiver [4], most often with a thermal source and optical chopping. The advantage of these systems is that they are low cost and easy to implement.

However, vector (i.e., coherent) beam pattern measurements of both amplitude and phase can offer a complete characterization of the optical system. Scalar measurements using a thermal source are broadband, which "smear out" standing waves and diffraction effects, for example, by a beam clipping the window of a cryostat. These effects are immediately noticeable in vector beam scans. A vector beam measurement characterizes the beam emerging from the last optical element, which is influenced by all optical elements preceding it. If the optical system is characterized well enough (i.e., amplitude and phase distortion per element), a vector beam scan can differentiate between errors in the fundamental beam provided by the detector, alignment errors in the optical system, or misalignment of the beam measurement system to the optical axis [5]. Furthermore, vector measurements are required to deconvolve the beam produced by the source probe from the measured field, which is a common practice since the source probe's beam makes the receiver beam appear larger than it should be if it is highly directive. Measuring the phase is also a key to compensate for standing waves and multiple reflections in the optical system, which are very common and usually a dominant source of error for heterodyne beam pattern measurements.

At submillimeter wavelengths, it is often impractical to be in the near field of the primary beam emerging directly from the detector, but it is almost impossible to be in the far field of

Manuscript received June 21, 2016; revised August 12, 2016; accepted September 27, 2016. Date of publication November 10, 2016; date of current version January 12, 2017. This work was supported in part by ERC starting Grant ERC-2009-StG and Grant 240602 TFPA. The work of K. K. Davis was supported in part by the Balloon-Borne Large Aperture Submillimeter Telescope—BLAST under the direction of National Aeronautics and Space Administration ROSES Grant NNX13AE50G.

K. K. Davis is with the School of Earth and Space Exploration, Arizona State University, Tempe, AZ 85287 USA (e-mail: kdavis32@asu.edu).

W. Jellema, S. J. C. Yates, and L. Ferrari are with the SRON Netherlands Institute for Space Research, Groningen 9747, The Netherlands (e-mail: w.jellema@sron.nl; S.Yates@sron.nl; l.ferrari@sron.nl).

J. J. A. Baselmans is with the SRON Netherlands Institute for Space Research, Utrecht 3584, The Netherlands, and also with the Terahertz Sensing Group, Delft University of Technology, Delft 2628, The Netherlands (e-mail: J.Baselmans@sron.nl).

K. Kohno is with the Institute of Astronomy, University of Tokyo, Tokyo 181-0015, Japan, and also with the Research Centre for the Early Universe, University of Tokyo, Tokyo 113-0033, Japan (e-mail: kkohno@ioa.s.u-tokyo.ac.jp).

D. Thoen is with the EEMCS Faculty, Microelectronics Department, Delft University of Technology, Delft 2628, The Netherlands (e-mail: d.j.thoen@tudelft.nl).

V. Murugesan is with the SRON Netherlands Institute for Space Research, Utrecht 3584, The Netherlands (e-mail: V.Murugesan@sron.nl).

A. M. Baryshev is with the SRON Netherlands Institute for Space Research, Groningen 9747, The Netherlands, and also with the Kapteyn Astronomical Institute, University of Groningen, Groningen 9700, The Netherlands (e-mail: a.m.baryshev@sron.nl).

Color versions of one or more of the figures in this paper are available online at http://ieeexplore.ieee.org.

Digital Object Identifier 10.1109/TTHZ.2016.2617869

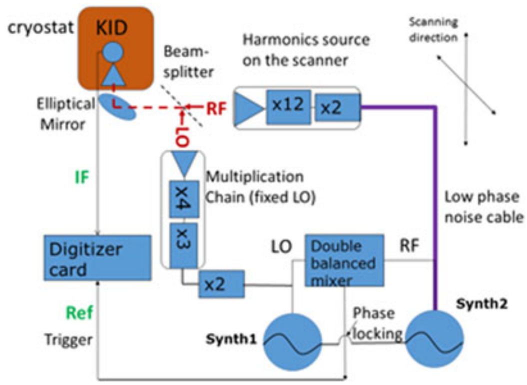

Fig. 1. Schematic of system components used in this experiment. The high frequency is labeled in red and the low frequencies are indicated in green.

TABLE I
EXPERIMENT SYSTEM FREQUENCIES

Location	f
Synth. 1	14.166500000 GHz
Synth. 2	14.166500400 GHz
RF	339.995009600 GHz
LO	339.995000000 GHz
IF	9600 Hz
Reference	400 Hz

List of the frequencies used for the heterodyne beam scanning system outlined in Fig. 1.

the primary mirror of a telescope system. This is especially true considering the state-of-the-art output power from sources in this wavelength regime, along with the attenuation through the atmosphere at long distances. Measuring amplitude and phase allows the E-field of the receiver to be propagated and then recreated at any distance z along the optical axis. This eliminates the necessity of taking multiple scans at different path lengths to trace the divergence of the beam angle, and the need to be in the far-field of the system as would be required with scalar measurements. Importantly, vector measurements allow full characterization of astronomical instruments at arbitrary points in their optical systems, including in the near field, for instruments where a far-field measurement may be inconveniently far from the receiver to be tested *in situ*. This technique could be of practical use for characterization of end-to-end optical systems based upon direct (incoherent) radiation detectors.

II. Methodology

Vector beam pattern measurements require at least one coherent source to illuminate the receiver. For amplifier-based detector systems, only one source is necessary, but for heterodyne instruments a local oscillator (LO) is also required. The LO may be injected optically as a second source located in the optical path of the receiver or may be injected directly with a waveguide hybrid. The measurement system used for this experiment is shown in Fig. 1 and is typical of a heterodyne beam scanning system requiring quasi-optical LO injection (see [6], [7]), except where noted in this section.

The two sources are frequency offset by a small value Δf, measured in Hertz, and are coupled together with a beamsplitter in the foreground of the receiver. The LO is stationary while the source signal is mounted on an *X*/*Y* motion stage. The signal of the detector read-out system is modulated at the difference of the two frequencies, according to (1), where we ignore terms outside the detector read-out bandwidth

$$S_{\mathrm{RO}} \propto E_{\mathrm{sig}} E_{\mathrm{LO}} \cos\left(2\pi\left(f_{\mathrm{sig}} - f_{\mathrm{LO}}\right)t + \Delta\varphi\right). \quad (1)$$

In this equation, S_{RO} is the complex signal recorded by the read-out system used, E_{sig} and E_{LO} are the electric field amplitudes of the input signal and LO sources, f_{sig} and f_{LO} are the signal and source frequencies, t is the time, and $\Delta\varphi$ is the relative phase shift between the two signals. The two signal input frequencies are related by $f_{\mathrm{sig}} = f_{\mathrm{LO}} - \Delta f$. The emerging signal modulated at the intermediate frequency, $\Delta f = f_{\mathrm{IF}}$, is then amplified and digitized. For MKIDs, $S_{\mathrm{RO}} = \theta_{\mathrm{MKID}}$, where θ_{MKID} is the phase of the complex in-phase and quadrature (IQ) signal used as the data acquisition (DAQ) technique for this experiment.

The source signal is scanned in front of the MKID in either a planar, cylindrical, or spherical pattern. The amplitude and phase response of the detector changes as a function of position relative to some set point in the measurement, usually the grid center thereby mapping the beam pattern of the device under test (DUT). The complex measurement field can be transformed into the radiation pattern of the receiver system. The frequencies used in this demonstration are shown in Table I. A more detailed description of the heterodyne measurement theory can be found in [8] and [9].

Instead of a true IF signal, the total power incident on the detector is modulated at the IF frequency, which translates to phase modulation of the IQ read-out signal θ_{MKID}. Our measurement scheme differs from a traditional system by recording a timeseries of the complex θ_{MKID} signal and taking a fast Fourier transform (FFT) to calculate the magnitude and phase of the modulation. They key focus of this paper is how to track the phase response of phase-insensitive detectors as the source probe is scanned through the measurement plane. We do this by recording the phase offset between θ_{MKID} and a reference signal via triggered acquisition. We create the reference by splitting the signal from the LO and source probe synthesizers at low frequency, combining them with a double-balanced harmonic mixer, and then feeding that signal as a trigger into the DAQ module. DAQ of the detector IF signal happens only after a positive zero crossing of the reference signal.

Fig. 2 shows the timeseries recorded at the central grid location of our measurement plane, as well as the FFT of that series. The reference signal is at the same phase as the incoming radiation to the detector, and any phase offset must, therefore, be caused by the phase delay of the Gaussian beam of the MKID. Thus, the relative phase offset of the detected signal to the reference signal encodes the phase response of the KID detector. In order to Nyquist sample the modulated MKID signal, the DAQ system must have a sampling rate of at least $2 * f_{\mathrm{IF}}$. In principal,

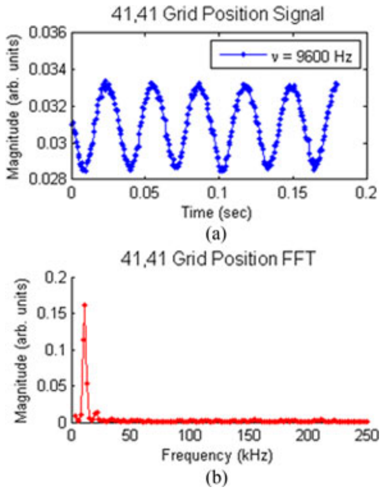

Fig. 2. Timeseries measurement of the amplitude of the IQ detector output at the central location in the measurement scan (a) and FFT (b). The IQ is modulated at 9600 Hz.

$f_{\rm IF}$ can be any positive value of Hertz. Practical limitations for $f_{\rm IF}$ are the read-out rate of the DAQ, especially for arrays with multiplexed readout schemes. $1/f_{\rm IF}$ must also be longer than the response time of the superconducting KID resonator. Lower values for $f_{\rm IF}$ may be used for devices with a slow response time, but higher offset frequencies decrease the $1/f$ noise in the system.

III. Experimental System

The DUT in this experiment was a meandering $\lambda/4$ hybrid Al-NbTiN superconducting KID, similar to the device in [10] except using a sapphire substrate instead of silicon. We tested a single pixel of a 4×4 array for which the DUT was centered geometrically within the system. The detector was fed by a twin-slot antenna that sits beneath a 2-mm-diameter laser-machined silicon lens array coupled to the device substrate. This new KID architecture is highly experimental and these are the first measurements of this new device.

The array was mounted within a dual stage ^{4}He–^{3}He cryostat reaching 250 mK. The cold optics consisted of a Gaussian beam telescope (see, for example, [11]) made of two hyperbolic high-density polyethylene lenses of focal length 25 mm and separated by twice the focal distance. One lens was directly mounted on the array housing and another was mounted to the 4-K shield. An optically limiting aperture (cold stop) was placed in between the lenses, limiting the opening angle to an $f/2$ beam, or 14° half opening angle.

The use of an elliptical mirror with a short focal length and low f-number optics led to significant off-axis aberrations, compounded by a slight cold defocus. There was misalignment between the two lenses due to curvature in the 4-K plate, which also caused misalignment to the elliptical mirror of order 3 mm. For these reasons, the position of the elliptical mirror was adjusted to give the most symmetric 3-dB beam shapes for all pixels, trading the on-axis aberration performance for better off-axis performance. A system diagram is shown in Fig. 3.

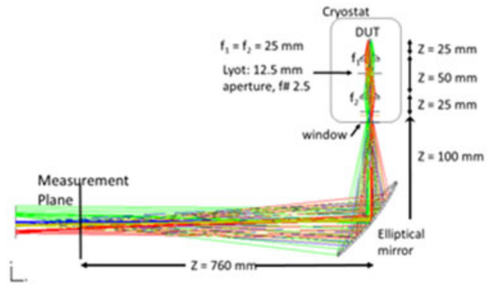

Fig. 3. Optical system schematic of the ^{4}He–^{3}He cryostat.

We use a modified ALMA band 9×24 chain as the stationary LO source [12]. The signal source was a harmonic generator based on a superlattice electronic device set to maximize the output power of the 12th harmonic of the input frequency [13], which was fed by an active frequency doubler. The spectral content of this device was checked with a Michelson Fourier transform spectrometer to ensure there were no harmonics within the bandpass of the receiver. A low-phase noise cable connected the scanned source to the synthesizer.

The system uses a homodyne detection technique to measure the changes in transmitted phase of a microwave readout signal that passes through a feedline coupled to the MKID. The readout system used for this experiment is summarized in [3]. We used DAQ rate of 500 kS/s, which limited our Nyquist sampling frequency to 250 kHz. At each point in the scan plane, a 300 point timeseries was acquired, and then 80 timeseries were averaged to produce the signal shown in Fig. 2(a). The phase and amplitude are taken from the peak in the FFT of the timesereis signal, shown in Fig. 2(b). The reference frequency of 400 Hz was chosen to ensure the modulation at high frequency (9.6 kHz) fell sufficiently below the Nyquist limit and the response time of the MKID at ~30 kHz.

With this experimental system, simultaneous measurement of the beam patterns of multiple KID detectors in an array configuration should be possible, with a multiplexing acquisition system and appropriate reimaging optics as necessary. This proof-of-concept demonstration used only a single pixel for simplicity of the system configuration and computational processing. In principle, there is no difference in the measurement system between scans of a single pixel or a whole array.

IV. Results

A. Device Linearity

We measured the linearity of the DUT by making a series of cuts across the measurement plane varying the input power to the signal source such that the DUT output power was reduced. In each cut, we measure the same beam pattern across a relative output power range of 50 dB. The detected power scans are shown in Fig. 4(a) on a logarithmic scale for different source input power levels. We note that the shape of the central lobe of the beam pattern remains the same for significantly different test source power levels, demonstrating excellent linearity of the KID. By comparing the measured cuts at low-power levels, one can accu-

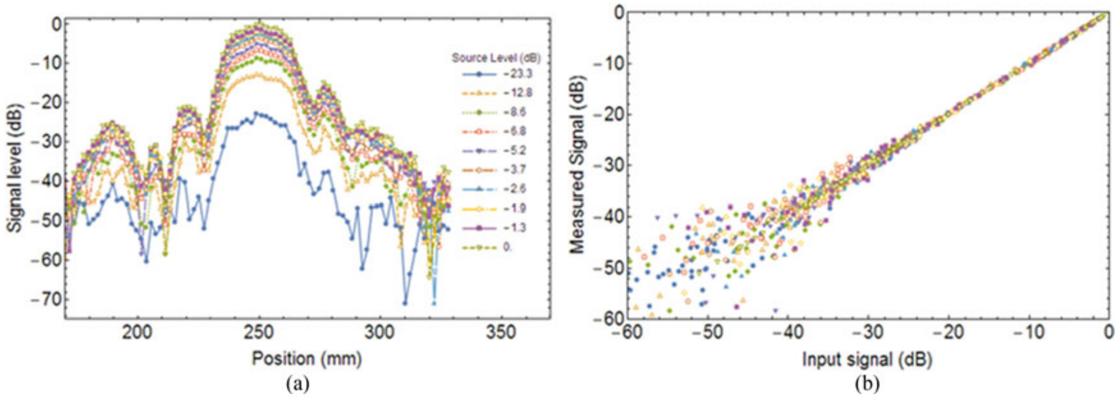

Fig. 4. Amplitude response of the receiver taken multiple times over the same *X* cut while varying the source probe input power (a). (b) Compares the input power to output power for each scan. We see there is excellent agreement for input signals greater than ~40 dB, showing that at peak center, the device is linear until the noise floor is reached at the edges of the scan.

rately determine the source power of each cut. This subsequently allows the recovery of the linearity plot of the system shown in Fig. 4(b). The power to drive the source is insufficient under 17.3 dBm. For the beam scans presented in this paper, the source power was kept at 17.5 dBm for maximum stability and signal-to-noise ratio corresponding to the -1.3 dBm line in Fig. 4.

B. Vector Maps

The amplitude and phase maps of the data collected using the above systems are presented in Fig. 5. The upper two scans were taken at a fixed distance from the cryostat, whereas the lower two scans were obtained by displacing the source by a distance of $\lambda/4 = 220\ \mu\text{m}$ from the original measurement plane. This axial offset was introduced to compensate for the effects of standing waves, as will be discussed in Section III-C. The Gaussian beam can be clearly recognized in Fig. 5(a) and (c), and panels (b) and (d) reveal the spherical phase fronts of the diverging beams as the phase increases from the phase center outward. The annular structure is caused by phase jumps where the phase wraps from $-\pi$ to $+\pi$. We have achieved a ~30-dB dynamic range in the amplitude scans. The phase data degrade where the noise floor is reached in the amplitude maps, indicating that the signals are strongly correlated.

C. Standing Wave Compensation

Monochromatic measurements are particularly susceptible to standing waves, where reflections can either constructively or destructively interfere with the incoming signal and cause a rippling effect in the beam pattern. We find a strong standing wave ripple effect discernable in these measurements. To correct for this, we employ the quarter-wave offset technique, available only for vector measurements. The technique involves taking two measurements of the E-field at the same *x, y* position in the scan, but offset by a quarter wave in *z*. The two maps are then coadded using the equation

$$s_c = \frac{s_1 + s_2 e^{-i\pi/2}}{2} \tag{2}$$

where s_1, s_2 are the complex signals taken at each distance *z*, and s_c is the compensated signal. When the two maps are coadded, a wave travelling parallel to the optical axis will have a phase shift of π/2, but a standing wave, traveling twice the distance, will have a phase shift of π. These waves will cancel each other to first order, effectively smoothing out the standing waves in the compensated map. A more detailed description of this technique can be found in [14].

Fig. 6 shows the central E-plane and H-plane cuts through the measured data, illustrating that the compensated signal is much smoother than either the $\Delta z = 0\,\mu\text{m}$ or $\Delta z = 220\,\mu\text{m}$ maps. For this demonstration, we manually moved the source probe for the *z*-offset with a micrometer mounted to the *X*/*Y* stage. Signal stability between the two maps could be increased by using a *XYZ* scanner that automatically takes the offset data before system drifts significantly.

V. Gaussian Beam Analysis

A. Gaussicity

We calculate the Gaussicity of the receiver's beam to be 80.3% by performing a normalized overlap integral (3) for the best-fit fundamental Gaussian mode $\psi_{0,0}$ (4) [11], [14]. The fitting algorithm used here produces an idealized Gaussian beam at the focal plane of the optical system, propagates the idealized beam to the measurement plane, and fits for the beam parameters that provide the best Gaussian beam coupling to the receiver's complex field at the measurement plane E_m. The overlap integral determines the degree of coupling between the measured complex field and that produced by $\psi_{0,0}$. The fitted parameters of the location of the focal plane and the idealized beam parameters are summarized in Table II. We predict a Gaussian beam coupling efficiency of 85% based on antenna-lens simulations, so we determine that the optical system scatters 5% of the incident lens-antenna beam into higher order modes.

We correct for any offsets in the measurement system by using a Nelder–Mead minimization algorithm to produce a primary beam in a new coordinate system with translational and rotational offsets to the measurement plane [15]. The translational offsets are characterized by *x-offset*, *y-offset*, and *z-offset*,

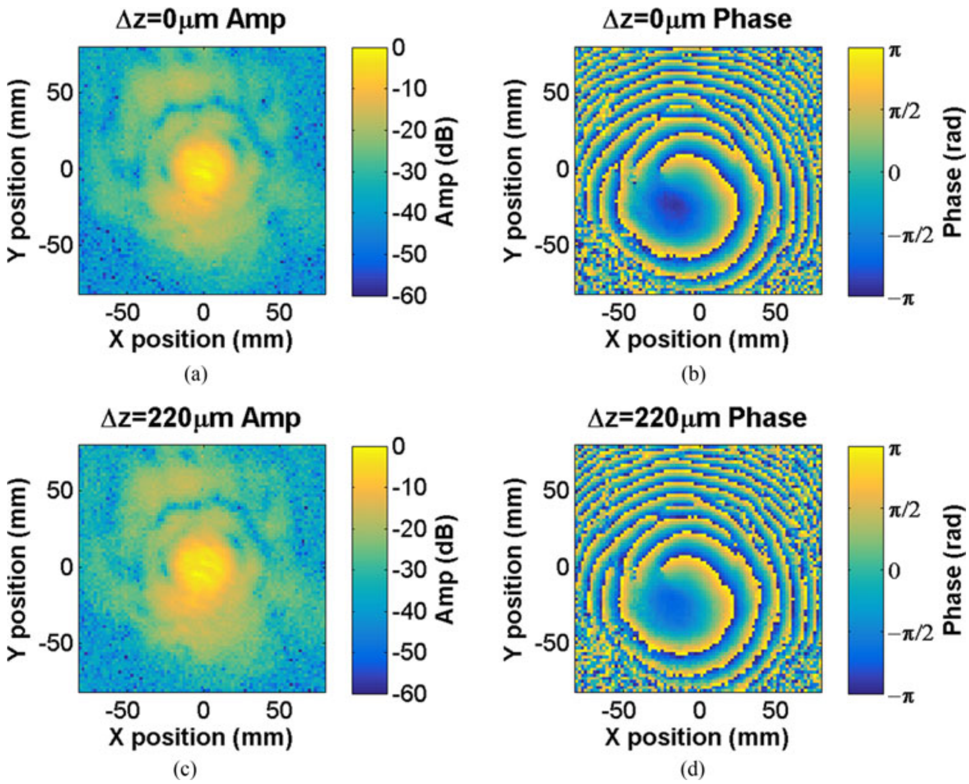

Fig. 5. Amplitude (a), (c) and phase (b), (d) measurements of the beam pattern of the KID receiver. The top two panels (a), (b) are the measurement with zero z offset, and the bottom two (c), (d) were taken after the scanned source was shifted by a distance of $z = 220\,\mu\mathrm{m}$.

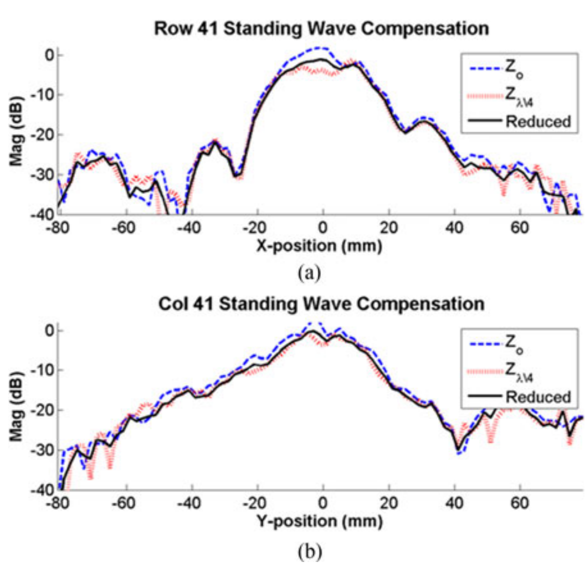

Fig. 6. X-cut (a) and Y-cut (b) of the standing wave reduced amplitude map. The red and blue lines show the two cuts at $\Delta z = 0\,\mu\mathrm{m}$ and $\Delta z = 220\,\mu\mathrm{m}$, respectively, and the solid black line is the reduced amplitude.

TABLE II
GAUSSIAN BEAM PARAMETERS

	Fit
Coupling Coefficient (unitless)	0.803
Coupling Loss (%)	19.7
$\omega_{o,x}$	11.6
$\omega_{o,y}$	10.0
$\Delta z_{x,y}$	−0.16
x-offset	−10.0
y-offset	−20.0
z-offset	600
θ_{Eul1} (rad)	0.028
θ_{Eul2} (rad)	−0.017
θ_{Eul3} (rad)	0.16

Gaussian beam parameters and coordinate system transformation values minimized to produce an optimal model Gaussian beam from the measurement data. All values given in mm unless otherwise stated.

and the rotational offsets are characterized by the Euler rotation angles θ_{Eul1}, θ_{Eul2}, θ_{Eul3}, and are shown in Fig. 7. The Gaussian beam parameters ω_x, ω_y, R_x, R_y, φ_x, φ_y are all dependent on the z' coordinate, and so are transformed to the primed coordinate system before being fit by the minimization algorithm, whereas the parameters $\omega_{0,x}$, $\omega_{0,y}$, and $\Delta z_{x,y}$ are independent in the unprimed coordinate system.

The minimization algorithm yields the lowest coupling loss by fitting for the independent Gaussian beam parameters and the offsets between the two coordinate systems. Our Gaussian beam function also accounts for any astigmatism in the beam by including an offset value $\Delta z_{x,y}$ between the phase centers in the $\hat{x}$- and $\hat{y}$-directions

$$c_c = \frac{\iint E_m\ \psi^*_{0,0}\delta x'\delta y'}{\iint |E_m|^2\delta x'\delta y' \iint |\psi_{0,0}|^2\delta x'\delta y'} \tag{3}$$

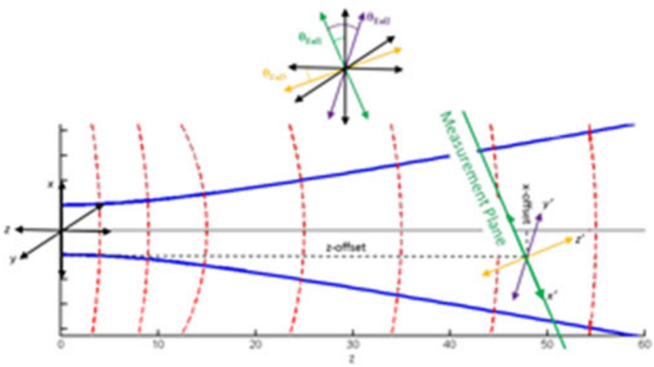

Fig. 7. Demonstration of a Gaussian beam in a reference frame *x, y, z*, and a measurement plane with a misaligned coordinate system x', y', z'. The idealized Gaussain beam parameters must be transformed from the x', y', z' to the *x, y, z* system before the overlap integral can be performed. The blue lines show the beam amplitude, and red dashed lines show the spherical phase fronts. The primed and unprimed coordinate systems are shown in relation to their origin and are also superimposed at the top of the figure.

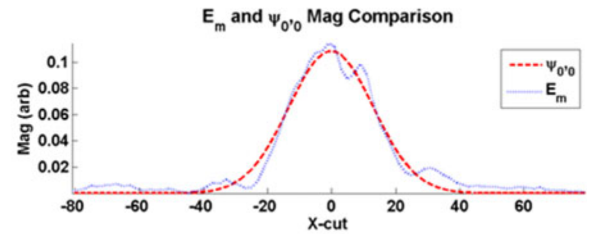

(a)

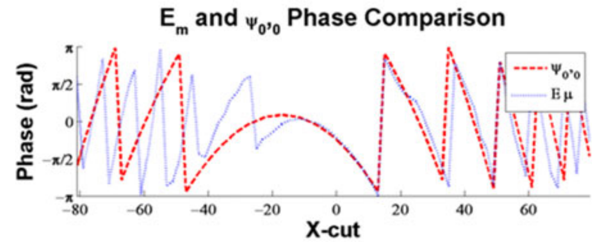

(b)

Fig. 8. Comparison of the central H-plane cut of the measured field E_m to the fitted Gaussian $\psi_{0,0}$ in amplitude (a) and phase (b).

where

$$\psi_{0,0} = \sqrt{\frac{2}{\pi\omega_x\omega_y}}\exp\left[-\left(\frac{x'^2}{{\omega_x}^2}+\frac{y'^2}{{\omega_y}^2}\right)-i\pi/\lambda\left(\frac{x'^2}{R_x}+\frac{y'^2}{R_y}\right)\right.$$
$$\left.-ikz+i/2\left(\phi_x-\phi_y\right)\right]. \quad (4)$$

A beamwaist of $\omega_{o,x} = 11.6$ and $\omega_{o,y} = 10.0$ mm gives a beam angle emerging from the elliptical mirror of 1.4°, 1.6°, respectively. This is consistent to first order with the beam angles derived separately from the angular plane wave spectrum (APWS) maps, where we find $\theta_x = 1.15°$ and $\theta_y = 1.09°$. The fitted tilt angles θ_{Eul1}, θ_{Eul2} are also fully consistent with the peak offset of the APWS map (see Section V-I). We believe the slight astigmatism is caused by errors introduced by the cold optical system in the cryostat and not introduced by misalignment of the beam measurement system as our analysis should remove these effects. Fig. 8 shows that the measured beam is well characterized by $\psi_{0,0}$ in amplitude, and our dominant error is in the phase matching.

We believe that there are significant optical effects arising from the specific architecture of the DUT, which may include a standing wave on the device substrate and misalignment of the lens antenna. A complete and qualitative comparison of the measured and expected optical performance of this device requires full characterization and control of the optical system geometries involved to within fractions of a wavelength. It also requires rigorous electromagnetic modeling of the preliminary and experimental lens-antenna system, which will not be available until the physical nature of the device is better understood and constrained, which was not the primary purpose of this experimental demonstration. A methodical characterization of the optical performance of this new device is suggested for follow-up research but lies beyond the scope of this paper.

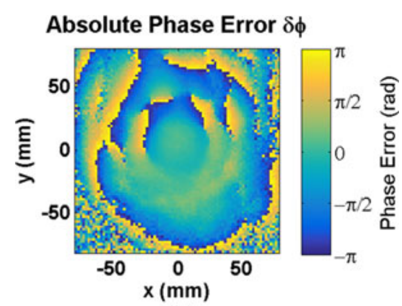

(a)

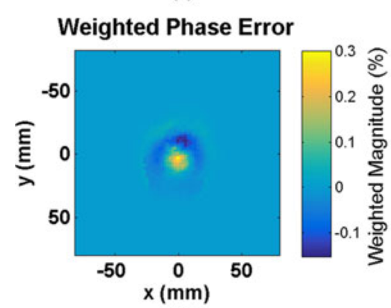

(b)

Fig. 9. Absolute phase error (a) and phase error weighted by the magnitude of the standing wave compensated amplitude measurement convolved with the ideal Gaussian beam propagated to the measurement plane (b). The phase error describes spherical aberrations of the phase fronts of the measured complex E field.

B. Wavefront Error

The divergence of the measured phase front from spherical is the best diagnostic tool for beam characterization. We have calculated the absolute and weighted residual phase error of the measured beam relative to the idealized beam, shown in Fig. 9. In the absolute phase error in Fig. 9(a), we see that the error is smooth for a significant distance from phase center demonstrating the phase is well-matched over the main peak of

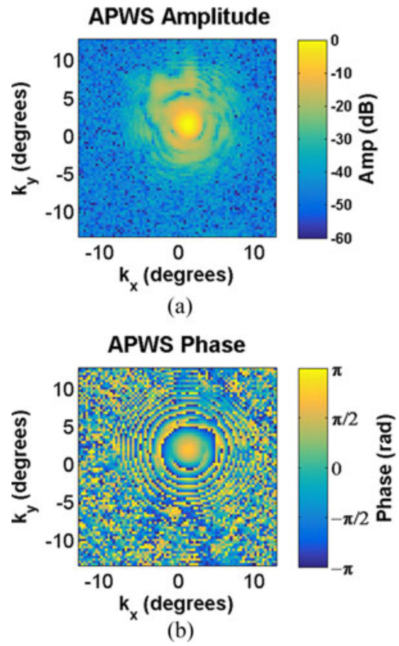

Fig. 10. Paraxial far field of the measured data. Amplitude is shown in (a) and phase is shown in (b). The phase is clearly recovered by the transformation. The signal degradation in the phase measurement traces the low signal in the amplitude measurement.

the beam. This is also conveyed in Fig. 8. In the weighted error plot in Fig. 9(b), we see even at the peak at phase center, the phase error is a fraction of a wavelength.

The phase behavior of the receiver is more sensitive to misalignment of the optical components of a system and to standing waves and multiple reflections than the amplitude response of a detector. The additional availability of simultaneously recorded phase and amplitude patterns tightly constrains the optical properties of the system under investigation. The optical errors we find in these measurements are indiscernible in the amplitude measurements (see Figs. 6 and 9), demonstrating the power of vector radiation pattern measurements as a diagnostic tool in detailed receiver characterization employing direct detectors.

VI. Angular Plane Wave Spectrum Analysis

One of the greatest advantages of the vector beam measurement technique is the ability to propagate the beam at the measurement plane either back through an optical system or outwards into the far field of the detector. This can be done by the technique of Huygens–Fresnel [16] principal or by angular plane-wave expansion [17]. The latter technique involves taking a 2-D Fourier transform of the field to create an APWS of the measured field. This APWS can be easily propagated through free space and recreate the field any distance z, positive or negative, along the optical axis. Fig. 10 shows the plane-wave spectrum amplitude and phase plots for this dataset. We retain signal-to-noise ratio of $\sim$30 dB. The APWS map has recovered the spherically symmetric phase structure. The peak offset in the APWS amplitude is in excellent agreement with the fitted Gaussian beam tilt angles, listed in Table II, both in sign as well as magnitude, illustrating that the key optical system properties can be consistently extracted from a single vector beam map.

VII. Conclusion

In this paper, we have unambiguously demonstrated a vector measurement technique using a MKID detector, which is in principle suitable for any direct detector instrument. This new technique provides measurement accuracy suitable to determine the primary beam characteristics of interest for receiver characterization. The phase preservation through APWS analysis, agreement to the predicted Gaussicity, and the agreement between the beam angles and derived from the overlap integral analysis and the APWS analysis verifies the system reliability.

Though vector beam measurements have an increase in cost and complexity in electrical components compared to scalar measurements, the advantage in the capability of performing multiple diagnostic tests from a single scan and making the required scan area significantly smaller make this measurement technique. Importantly, a single scan at a fixed position in z simultaneously finds the beamwaist and focal position of the receiver. We will continue this work by understanding the optical performance of each element in the receiver chain and completing the analysis of the end-to-end system, with detailed comparisons of the measurement to electromagnetic simulations. Follow-up work for other instrument analyses is already underway to take this system and use it as a diagnostic tool both from a device and an instrument perspective, as well as scaling the analysis pipeline to measure a full detector array.

Acknowledgment

The authors would like to thank A. Endo for use of a multiplier chain. The authors would also like to thank A. Khudchenko, J. Barkhof, and the NOVA ALMA group for support and use of a multiplier chain and harmonic mixer. Author K. K. Davis would like to thank C. Groppi for his guidance during this analysis.

References

[1] J. Zmuidzinas, "Superconducting microresonators: Physics and applications," *Annu. Rev. Cond. Matter Phys.*, vol. 3, pp. 169–214, Mar. 2012.

[2] J. Baselmans, "Kinetic inductance detectors," *J. Low Temp. Phys.*, vol. 167, no. 3, pp. 292–304, May 2012.

[3] P. K. Day, H. G. LeDuc, B. A. Mazin, A. Vayonkias, and J. Zmuidzinas, "A braodbans superconducting detector suitable for use in large arrays," *Nature*, vol. 425, pp. 817–821, Oct. 2013, doi:10.1038/nature02037.

[4] S. J. C. Yates *et al.*, "Clean beam patterns with low crosstalk using 850 GHz microwave kinetic inductance detectors," *J. Low Temp. Phys.*, vol. 176, no. 5, pp. 761–766, Sep. 2014.

[5] W. Jellema *et al.*, "The HIFI focal beam characterization and alignment status," in *Proc. 19th Int. Symp. Space THz Technol.*, Apr. 2008, pp. 448–455.

[6] M. Naruse, M. Kamikura, Y. Sekimoto, T. Ito, M. Sugimoto, and Y. Izuka, "Near-field beam and cross-polatization pattern measurement of ALMA band 8 cartridges," in *Proc. 19th Int. Symp. Space THz Technol.*, Groningen, The Netherlands, 2008, pp. 534–539.

[7] C. Tong, S. Paine, and R. Blundel, "Near-field characterization of 2D beam patterns of sub-mm superconducting receivers," in *Proc. 5th Int. Symp. Space THz Technol.*, Ann Arbor, MI, USA, May 1994, pp. 660–673.

[8] A. Yaghjian, "An overview of near-field antenna measurements," *IEEE Trans. Antennas Propag.*, vol. 34, no. 1, pp. 30–45, Jan. 1986, doi: 10.1109/TAP.1986.1143727

[9] R. Johnson, H. Ecker, and J. Hollis, "Determination of far-field antenna patterns from near-field measurements," *Proc. IEEE*, vol. 6, no. 12, pp. 1688–1694. Dec. 1973.
[10] R. Janssen *et al.*, "High optical efficiency and photon noise limited sensitivity of microwave kinetic inductance detectors using phase readout," *Appl. Phys. Lett.*, vol. 103, pp. 203503-1–203503-4, Nov. 2013.
[11] P. Goldsmith, "Gaussian beam propagation," in *Quasioptical Systems: Gaussian Beam Quasioptical Propagation and Applications.* New York, NY, USA: Wiley–IEEE Press, 1998.
[12] A. Baryshev *et al.*, "The ALMA band 9 receiver," *Astron. Astrophys.*, vol. 577, 2015, Art. no. A129, doi: 10.1051/0004-6361/201425529.
[13] D. G. Paveliev *et al.*, "Experimental study of frequency multipliers based on a GaAz/AlAs semiconductor superlattices in the terahertz frequency range," *Semiconductors*, vol. 46, pp. 121–125, 2012.
[14] W. Jellema, "Optical design and performance verification for Hershel-HIFI," Ph.D. dissertation, Univ. Groningen, Groningen, The Netherlands, 2015.
[15] J. A. Nelder and R. Mead, "A simplex method for function minimization," *Comput. J.*, vol. 7, no. 4, pp. 308–313, 1965.
[16] C. Balanis, "Aperture antennas," in *Antenna Theory: Analysis and Design*, 3rd ed. New York, NY, USA: Wiley, 2005.
[17] L. Novotney. (2013, Feb.). Angular Spectrum Representation. ETH Zürich, Photonics Laboratory. Zürich, Switzerland. Lecture Notes. [Online]. Available: https://www.photonics.ethz.ch/fileadmin/user_upload/Courses/EM_FieldsAndWaves/AngularSpectrumRepresentation.pdf

Kristina K. Davis received the B.A. degree in astronomy from the University of Colorado at Boulder, Boulder, CO, USA, in 2012, and is currently working toward the Ph.D. degree in exploration systems design (with a concentration in instrumentation) at Arizona State University, Tempe, AZ, USA.

Since becoming a graduate student in 2012, her work has been focused on the design, fabrication, calibration, and testing, and data analysis for astronomical missions in the THz frequency regime. She has lead the development of a feedhorn array for the Stratospheric Terahertz Observatory 2 Mission, and has participated in several instrument commissioning campaigns. Her research interests include design ground, atmospheric, and space-based instruments to study the lifecycle of the gas and dust in the interstellar medium. She also focuses on instrument characterization measurement systems, measurement strategies, and optical analysis.

Willem Jellema received the M.Sc. degree (*cum laude*) in applied physics from the University of Groningen, Groningen, The Netherlands, in 1998, and the Ph.D. degree (*cum laude*) in applied physics (on the optical design and performance verification of Herschel-HiFi) from the Faculty of Mathematics and Natural Sciences, University of Groningen, in 2015.

From 1998 to 2015, he was an Instrument Scientist on the Herschel-HIFI Project, responsible for the end-to-end optical design verification, alignment, and calibration. Since 1998, he has been with the SRON Netherlands Institute for Space Research, Groningen, where he is currently a Senior Instrument Scientist. Since 2009, he has been the Instrument Scientist of SPICA-Safari, a far-infrared spectrometer proposed for a large aperture cryogenic telescope in space. In 2014, he also became the lead Systems Engineer of SPEX, an optical multiangle spectropolarimeter for future atmospheric missions. He has been involved in various other projects related to the development, design, construction, verification, and calibration of submillimeter wave and optical instrumentation for space. His experience and research interests include system design, architecture and concept definition, system engineering, optics, performance analysis, modeling and experimental techniques, with a special interest in long-wave diffractive optics and coherent heterodyne technologies and applications.

Stephen J. C. Yates received the Ph.D. degree in experimental low-temperature techniques for condensed matter physics from the University of Bristol, Bristol, U.K., in 2003.

He was with the CNRS-CRTBT Grenoble, France, as a Postdoctoral Researcher, where he was involved with low-temperature magnetism, before moving into the development of low-temperature detectors for astrophysics again with the CNRS-CRTBT (now Institut Neél) Grenoble (2004–2006). He is currently an Instrument Scientist working on superconducting microwave kinetic inductance detectors (MKIDs) with SRON, The Netherlands Institute for Space Research, Groningen, The Netherlands, which he started in 2006. He has coauthored more than 40 peer-reviewed papers with personal highlights including submillimeter photon noise observation with MKIDs (*Applied Physics Letters* in 2011), MKID multiplexed readout (*Applied Physics Letters* in 2009), high-impedance bolometer multiplexed readout (*Review of Scientific Instruments* in 2007), and low-temperature magnetism (*Physical Review Letters* in 2003). His current research interests include MKID development for submilimeter applications including the underlying physics of MKIDs, MKID readout, novel applications of MKIDs, MKID characterization, and application in scientific instruments for the astronomical community.

Lorenza Ferrari received the Ph.D. degree in applied physics (working on cryogenic detectors for astrophysics applications), from the University of Genoa, Genova, Italy, in 2009.

She then worked for one year with the INFN Genoa and PTB Berlin, Germany, as a Postdoctoral Researcher on low-temperature detectors for neutrino mass experiments. Since 2010, she has been an Instrument Scientist with SRON, The Netherlands Institute for Space Research, Groningen, The Netherlands. Her current research interests include development of microwave kinetic inductance detectors for submilimeter applications and transition edge sensors for far-IR frequency range focusing on optical characterization and application in scientific instruments. She is also involved in the SpicA FAR-infrared Instrument and X-ray integral field unit spectrometer experiments modeling and testing the focal plane assembly as well as designing cryogenic facilities for performance validation of instruments components.

Jochem J. A. Baselmans was born in 1974. He received the Graduate degree and Ph.D. degree (*summa cum laude*) in controllable josephson junctions from the University of Groningen, Groningen, The Netherlands, in 1998 and 2002, respectively.

In 2002, he became a Postdoctoral Instrument Scientist with the SRON Netherlands Institute for Space Research, Groningen, where he worked until 2004 on hot electron bolometer mixers, very sensitive heterodyne radiation detectors for frequencies between 1 and 5 THz. In 2005, he joined SRON Utrecht and started working on microwave kinetic inductance detectors (MKIDs), after a three month visit to the California Institute of Technology, Pasadena, USA. He currently leads the Dutch effort on the development of MKIDs. He is currently a Senior Instrument Scientist with the SRON Netherlands Institute for Space Research, where since 2002, he has been with the Technology Division. Since 2015, he has been an Associate professor with the THz Sensing Group, Delft University of Technology, Delft, The Netherlands. He has authored or co-authored more 80 papers.

Dr. Baselmans was the recipient of an ERC Consolidator Grant to develop an advanced imaging spectrometer based upon MKIDs in 2015.

Kotaro Kohno was born in 1969. He received the Ph.D. degree in astronomy [on the observational study of dense intersteller medium in the central regions of nearby active galaxies using nobeyama millimeter array (NMA)] from the University of Tokyo, Tokyo, Japan, in 1998.

Until 2001, he was involved with the development of 230-GHz SIS receivers for NMA along with the operation of NMA and observational studies of molecules in galaxies near and far. He has also been involved with the construction and operation of the Atacama Submillimeter Telescope Experiment (ASTE) including the development of SIS receivers for ASTE. In 2001, he joined the Institute of Astronomy (IoA), Graduate School of Science, University of Tokyo, and he has been a Professor in the Radio Astronomy Group of IoA, Univeristy of Tokyo, since 2009. He is currently leading and involved with various research programs using atacama large millimeter/submillimeter array. His recent research interests include next-generation telescopes, superconducting devices and their application for ground-based millimeter and submillimeter astrophysics to understand the formation and evolution of galaxies, and supermassive black holes in the universe.

David Thoen was born in Nieuwveen, The Netherlands, in 1978. He received the B.S. degree in applied physics from the Fontys University of Technology, Eindhoven, The Netherlands, in 2008.

In 2007 he joined the Dutch Institute for Fundamental Energy Research (formerly known as FOM Institute Rijnhuizen), Nieuwegein, The Netherlands, as a Microwave Engineer working on microwave diagnostics for real-time control of electron-cyclotron resonance heating of nuclear fusion plasmas in tokamaks. In 2010, he joined the Cosmo Nanoscience Group, Delft University of Technology, Delft, The Netherlands, working on the development and fabrication of the band 9 (600–720 GHz) detector chips of the atacama large millimeter array. Since 2012, he has been working on microwave kinetic inductance detectors (MKID), and since 2015, he has been with the Terahertz Sensing Group, Delft University of Technology. He is responsible for the MKID processing in Kavli cleanroom at Delft with a focus on reactive sputtering of niobium–titanium–nitride and quality control of thin films. He has coauthored more than 20 papers.

Vignesh Murugesan received the M.Sc. degree in microsystem integration technology from the Chalmers University of Technology, Gothenburg, Sweden, in 2007.

He was a Process Integration Engineer from 2007 to 2008, with Infineon Technologies AG, Regensburg, Germany. From 2010 to 2013, he was a MEMS Process Engineer with Thermo Fisher Scientific, Enschede, The Netherlands. Since 2013, he has been a Process Engineer with the Microwave Kinetic Inductance Detectors Group, SRON Netherlands Institute for Space Research, Groningen, The Netherlands. He is currently responsible for the fabrication and process development of MKID chips.

Andrey M. Baryshev received the M.S. degree (*summa cum laude*) in physical quantum electronics from the Moscow Physical Technical institute, Moscow, Russia, in 1993, and the Ph.D. degree in superconducting integrated receiver combining SIS mixer and flux flow oscillatoron into one chip from the Technical University of Delft, Delft, The Netherlands, in 2005.

He is currently a Senior Instrument Scientist and has been with the SRON Low Energy Astrophysics Division, Groningen, The Netherlands, and Kapteyn Astronomical Institute, University of Groningen, Groningen, since 1998. In 1993, he was an Instrument Scientist with the Institute of Radio Engineering and Electronics, Moscow, involved in the field of sensitive superconducting heterodyne detectors. In 2000, he joined an effort to develop an SIS receiver (600–720 GHz) for the atacama large millimiter array, where he designed the SIS mixer, quasi-optical system, and contributed to a system design. His current main research interests include application heterodyne and direct detectors for large focal plane arrays in THz frequencies and quasi-optical systems design and experimental verification.

Dr. Baryshev was the recipient of the NWO-VENI Grant for his research on heterodyne focal plane arrays technology in 2008 and, in 2009, he was the recipient of the EU commission Starting Researcher Grant for his research on focal plane arrays of direct detectors.